



The Influence of Cooling Rate on Austenite Stability and Mechanical Properties in an Austenite–Ferrite Medium-Mn Steel

Zhihui Cai, Deliang Zhang, Guangqi Wen, Lifeng Ma, and R.D.K. Misra

Submitted: 21 December 2020 / Revised: 12 May 2021 / Accepted: 1 June 2021 / Published online: 28 July 2021

The impact of cooling rate on austenite stability and mechanical properties of a cold-rolled transformation-induced plasticity (TRIP) steel with nominal chemical composition of Fe-11Mn-4Al-0.2C (wt.%) was elucidated in the present study. Mechanical properties were obtained by tensile test and microstructure was analyzed by XRD, SEM, EMPA. Intercritical annealing in the range of 700–800 °C for 5min followed by either water-quenched or air-cooled, both led to a ferrite–austenite mixed microstructure. However, the austenite stability varied with the annealing temperature. The water-quenched and air-cooled samples annealed at 750 °C with medium austenite stability demonstrated significantly higher ductility than the samples annealed at 700 and 800 °C. The superior total elongation (TE) in 750 °C sample was not only contributed by TRIP effect of austenite, but also the cooperative deformation of ferrite. The air-cooled samples were characterized by higher austenite stability and ultimate tensile strength (UTS), but lower total elongation compared to the water-quenched samples, which is because the TRIP effect in the air-cooled samples without the cooperation of ferrite contributed primarily to work hardening and UTS, but less to TE. Moreover, the critical factor in controlling austenite stability of water-quenched sample was morphology, granular austenite showing the highest stability; while the dominant factor in austenite stability of the air-cooled sample was composition, enrichment of Mn and C improving austenite stability.

Keywords austenite stability, cooling rate, mechanical properties, medium-Mn steel, microstructure, TRIP effect

1. Introduction

Medium-Mn (4~12 wt.%) steels characterized by outstanding mechanical properties are receiving increased attention because they are considered as potential candidates for automotive applications. Comparing with conventional low-alloyed transformation-induced plasticity (TRIP) steels, medium-Mn steels have significantly higher fraction of austenite (>30%) which transforms into martensite during deformation and plays a role in stress transfer and reducing stress concentration, i.e., transformation-induced plasticity (TRIP) effect, contributes to superior mechanical performance (>30 GPa.%) (Ref 1-5)].

It is well accepted that TRIP effect is closely related with austenite stability. In order to achieve excellent strength–ductility balance, austenite should have appropriate stability and is transformed gradually over a large strain range rather than exhausted during the initial deformation stage, or retained

significantly prior to fracture. Austenite stability is dependent on various factors such as composition (Ref 6-8), grain size (Ref 4, 9), morphology (Ref 10, 11), and crystallographic orientation of austenite (Ref 12, 13), among which the composition and grain size are of particular significance parameters (Ref 8, 9).

In medium-Mn steels, metastable austenite can be obtained from martensite by austenite-reverted transformation (ART) heat treatment (Ref 14-16). In addition, austenite can be developed through the partitioning of austenite stabilizers, such as C and Mn through intercritical annealing (Ref 17). Han et al. (Ref 18) proposed that heating rate influenced reverse transformation mechanisms from martensite to austenite, leading to the variation in morphology and Mn concentration in austenite. Li et al. (Ref 14) compared ART heat treatment and quenching & tempering (Q&T) process on the austenite stability and mechanical properties in hot-rolled Fe-0.2C-1.6Al-6.1Mn TRIP steel and indicated that Q&T process enabled appropriate enrichment of elements and hence desired stability for significant TRIP effect, while austenite was too stable by ART process and deteriorated TRIP effect.

Therefore, a number of studies on the relationship between annealing conditions (temperature, soaking time, heating rate, etc.) and austenite stability have been performed (Ref 14, 17, 18). However, so far, studies of the effect of cooling rate on microstructural evolution and mechanical properties are limited. For example, Steineder et al. (Ref 19) reported that the variation of annealing temperature and cooling rate altered the amounts of ferrite, retained austenite, bainite, pearlite, and martensite in the final microstructure of Fe-0.1C-3.5/5Mn steel through dilatometric experiment and thermodynamical modeling. The present study is to investigate the influence of cooling rate and annealing temperature on austenite stability and

Zhihui Cai and Lifeng Ma, School of Mechanical Engineering, Taiyuan University of Science and Technology, Taiyuan 030024, China; Deliang Zhang and Guangqi Wen, School of Materials Science and Engineering, Northeastern University, Shenyang 110819, China; R.D.K. Misra, Laboratory for Excellence in Advanced Steel Research, Department of Metallurgical, Materials and Biomedical Engineering, University of Texas at El Paso, El Paso, TX 79968. Contact e-mail: mlf_zgtyust@163.com.

partitioning of elements. Additionally, the effect of cooling rate on work hardening behavior and mechanical property is elucidated.

2. Experimental

The exact chemical composition of experimental steel is 11.02Mn, 0.18C, 3.81Al and balance Fe in mass percentage (wt. %). The ingot was heated at 1200 °C for 2 h, hot forged into several rods with a section size of 100 mm×30 mm, and then air cooled to ambient temperature. Subsequently, the rods were subjected to eight-pass hot rolling in the temperature range of 850~1200 °C. Finally, the hot-rolled sheets with a thickness of 4 mm were cold-rolled to 1 mm thickness. According to our previous work (Ref 13, 20), the steel exhibited excellent mechanical property combinations when it was annealed in the two-phase region (700~800 °C), and there were no carbides due to high Al content. Thus, the cold-rolled sheets were heated at 700, 750, and 800 °C for 5 min, respectively, and then cooled in water or air. The cooling rate in water was between 200 and 400 °C/s, and cooling rate in air was between 3 and 5 °C/s.

Tensile tests were conducted on specimens of 12.5 mm width and gauge length of 25 mm, using a universal testing machine (SANSMT 5000) at a constant cross head speed of 3 mm·min⁻¹ at room temperature. Microstructural examination was carried out using scanning electron microscope (Ultra Plus FESEM) and electron probe microanalyzer (JEOL JXA-8530F), both at the condition of electrode parameter of 15KV EHT, 9.7mm WD. The samples were etched with 25% sodium bisulfite aqueous solution for 3~5 s. The specimens were polished with 10% perchloric acid + 90% alcohol by HY3005ET electropolisher, at the condition of electrode parameter of 20 V, 3.5 mA, 30 s, 25 °C. The volume fraction of austenite was determined by x-ray diffraction (Smartlab) with CuK_{α} radiation using direct comparison method (Ref 20), involving the use of integrated intensities of (200)_α and (211)_α peaks and those of (200)_γ, (220)_γ, and (311)_γ peaks. The volume fraction of austenite V_A was calculated using equation (Ref 21):

$$V_A = 1.4I_{\gamma} / (I_{\alpha} + 1.4I_{\gamma}) \quad (\text{Eq 1})$$

where I_{γ} is the integrated intensity of austenite and I_{α} is the integrated intensity of phases with body-centered cubic structure.

3. Results

3.1 Microstructure

Fig. 1 shows SEM micrographs of cold-rolled samples heated at 700, 750, and 800 °C for 5min, followed by water quenching. The microstructural constituents consisted of α-ferrite, δ-ferrite, and austenite. The two kinds of ferrite could be distinguished by their morphology. δ-ferrite was featured with strip-like and α-ferrite was equiaxed. The effect of α-ferrite and δ-ferrite on tensile properties was similar, which had been

proven in our previous work (Ref 22). The microstructure of austenite can be divided into three types: lamellar, granular, and blocky. The proportion of equiaxed microstructure and the grain size increased with the increase of annealing temperature. SEM micrographs of cold-rolled samples air cooled from 700, 750, and 800 °C, respectively, are presented in Fig. 2. Similarly, the microstructural constituents of the air-cooled samples comprised of ferrite and austenite. However, the air-cooled samples had a greater and more uniform grain size than water-quenched samples. Moreover, it seems that austenite fraction was different for the two groups and was confirmed by XRD.

The measured austenite fraction as a function of annealing temperature is summarized in Fig. 3. As illustrated in Fig. 3(a), in the case of water-quenched samples, the austenite fraction prior to the tensile test increases from 50.2% to 74.2% with the increase of temperature. In contrast, in air-cooled samples, the austenite fraction prior to the tensile test increases slightly and was ~70% (Fig. 3b). For the samples after tensile tests, the austenite fraction decreases significantly with increase in temperature, indicating the enhanced TRIP effect.

According to the previous study, the austenite fraction of Fe-11Mn-4Al-0.2C steel increased with increase in annealing temperature (Ref 13). In view of the short holding time (5min) at the annealing temperature, the α↔γ transformation did not occur adequately (Ref 23). It is inferred that dynamic α↔γ transformation occurred during cooling in air. According to the austenite–ferrite transformation dynamic model (Eq 2) (Ref 24):

$$X(t) = 1 - \exp(-\pi G^3 N t^4 / 3) \quad (\text{Eq 2})$$

where $X(t)$ is transformation fraction, N is nucleation rate, G is isotropic growth rate, N is constant, t is time. It is inferred that longer residence time in the two-phase region during cooling process is favorable to γ↔α transformation. Therefore, in the present work, the fraction and stability of austenite of water-quenched samples were only influenced by the annealing heat preservation stage, due to very fast cooling rate. In contrast, the fraction and stability of austenite of air-cooled samples were influenced by the annealing heat preservation stage and cooling period, due to slow cooling rate. Therefore, it is implied that α → γ transformation is more significant than γ → α transformation during air cooling from 700~750 °C to ambient temperature, while γ → α transformation played the dominant role during air cooled from 750~800 °C to ambient temperature.

3.2 Mechanical Properties

Figure 4(a) and (b) shows engineering stress–strain curves of water-quenched samples and air-cooled samples, respectively. The variation of tensile properties of the two sets of samples is similar. Yield strength (YS) decreases with increase in temperature because of the increase in grain size (as evidenced in Fig. 1), consistent with the Hall–Petch equation. The ultimate tensile strength (UTS) increases with increasing temperature, which is primarily attributing to enhanced TRIP effect during tensile deformation (consistent with Fig. 3a). However, it is intriguing that the total elongation (TE) reaches a maximum at 750 °C, and is greater than the other two temperatures, which could not be well explicated by TRIP effect, and will be discussed in the next section.

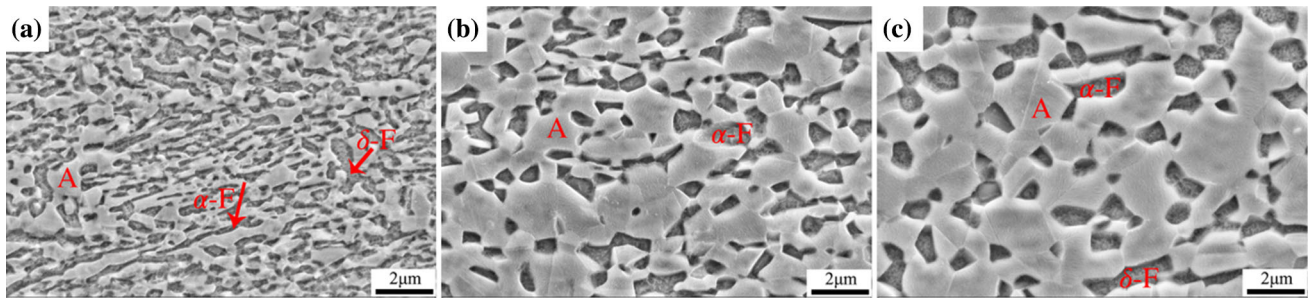


Fig. 1. Micrographs of the cold-rolled sample water quenched from different temperature. (a) 700 °C, (b) 750 °C, (c) 800 °C. (A: austenite, α -F: α ferrite, δ -F: δ ferrite)

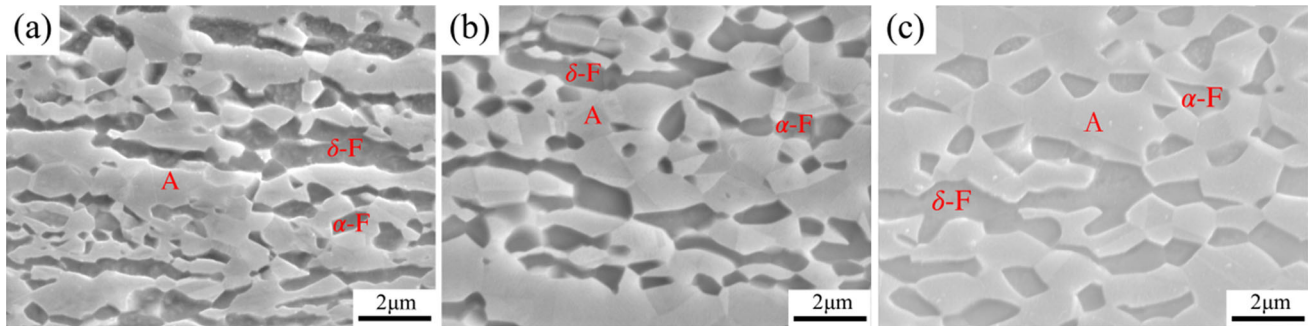


Fig. 2. Micrographs of the cold-rolled sample air cooled from different temperature. (a) 700 °C, (b) 750 °C, (c) 800 °C. (A: austenite, α -F: α ferrite, δ -F: δ ferrite)

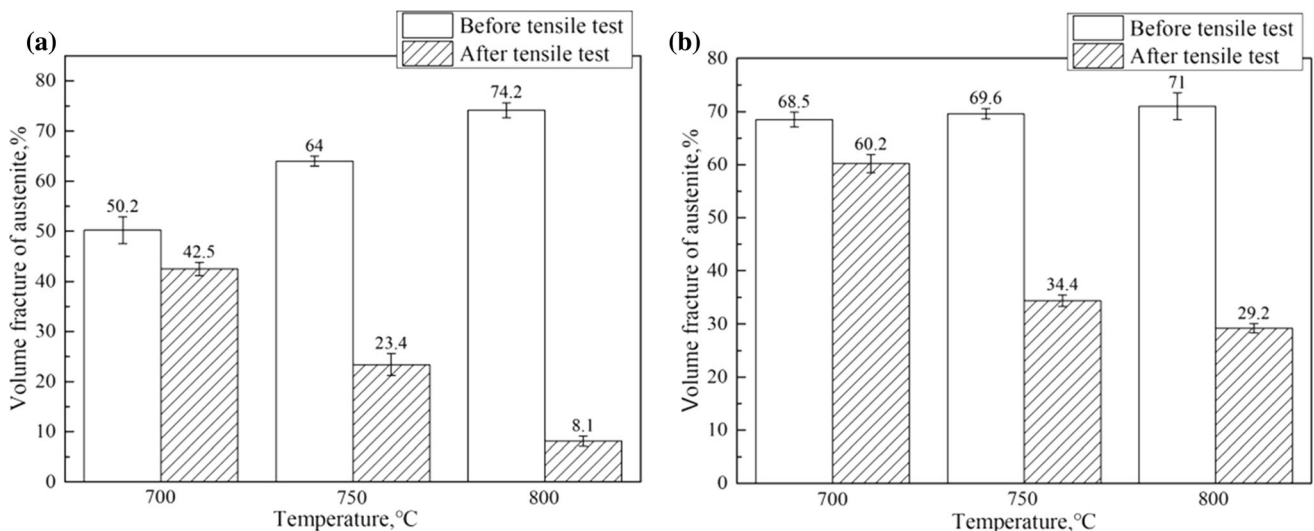


Fig. 3. Measured austenite fraction of the two sets of samples. (a) water-quenched samples, (b) air-cooled samples

4. Discussion

4.1 Tensile Behavior

Given that the two sets of samples have similar variation of tensile properties, we focus on the water-quenched samples. Fig. 5 shows the work hardening behavior of the samples water quenched from 700, 750, and 800 °C, respectively. The work hardening rate (WH) could be divided into three stages. The stage 1 of the three samples is similar, characterized by serration and corresponds to the discontinuous yielding plateau. However, stage 2 and 3 are different for the three samples.

According to the XRD results, TRIP effect was insignificant in 700 °C sample, leading to continuous decrease in WH and lower TE. In contrast, in the case of 800 °C sample, as illustrated in Fig. 5(c), WH increases quickly in stage 2, which is mainly associated with the TRIP effect. Moreover, WH fluctuating around a high value of 3300MPa in stage 3 is a consequence of discontinuous TRIP effect (Ref 25). Although 800 °C sample demonstrated the strongest TRIP effect (as evidenced in Fig. 3a), its TE (37%) was similar to that of 700 °C sample (38%), and much less than that of 750 °C sample (67%).

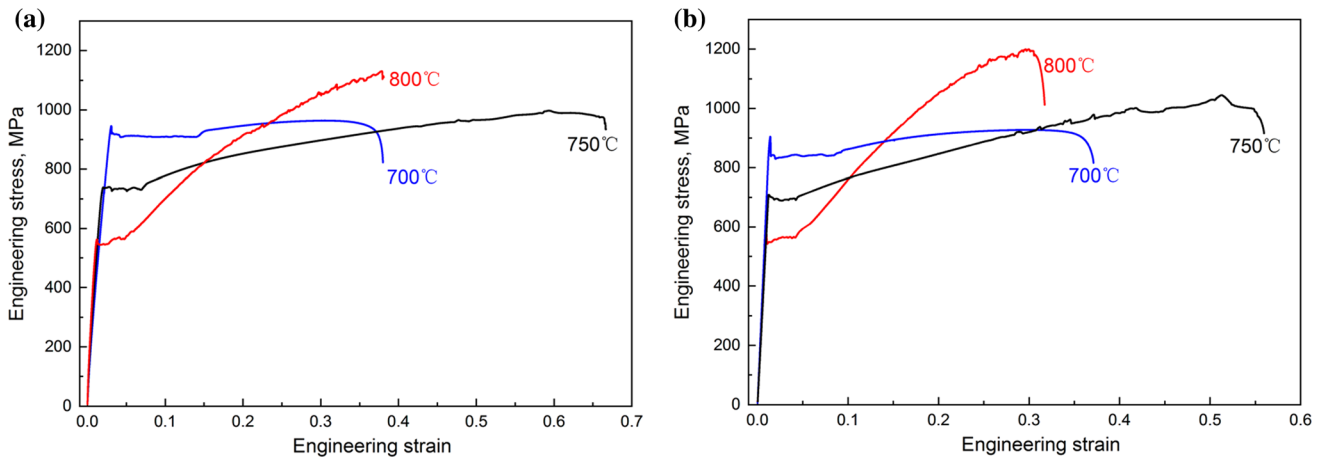


Fig. 4. Engineering strain–stress curves of the two sets of samples. (a) water-quenched samples, (b) air-cooled samples

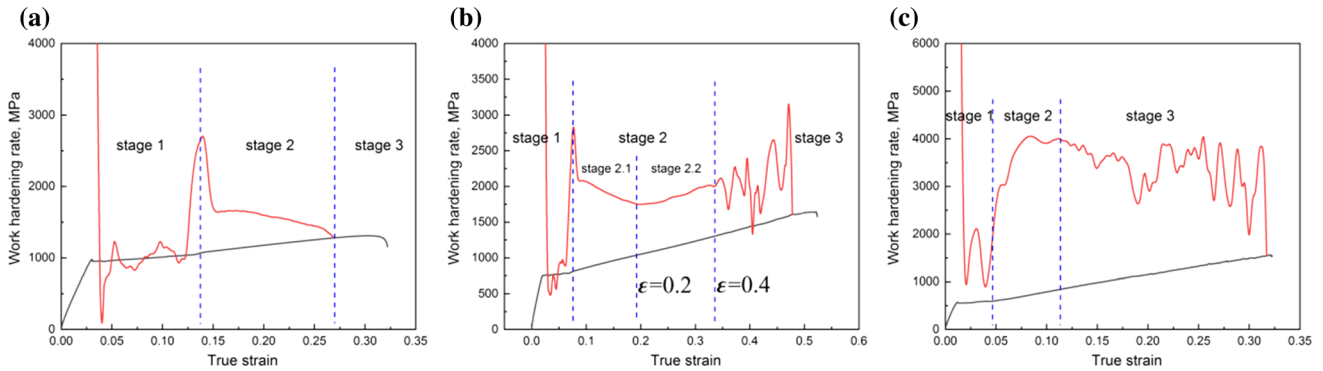


Fig. 5. True strain–strain curves and the corresponding work hardening rate of the samples water quenched from different temperatures. (a) 700 °C, (b) 750 °C, (c) 800 °C

To determine the contribution of TRIP effect to TE, 750 °C water-quenched sample was subjected to interrupted tensile test. Fig. 6 shows the variation of austenite fraction as a function of engineering strain. Due to austenite with different degree of stability, the fraction of martensite transformation is different during deformation. When the engineering strain was less than 0.2, the stress was so small that martensitic transformation could not be initiated, which resulted in insignificant TRIP effect, corresponding to a continuous decrease in WH (stage 2.1). When the engineering strain reached 0.2, the stress attained critical value and massive austenite with low stability transformed to martensite (austenite fraction decreased from 62.3% to 30.8%). However, it is intriguing that the corresponding WH in stage 2.2 increased slowly (Fig. 5b), indicating that the large amount of martensite transformation contributed little to WH. To interpret this strange phenomenon, microstructural evolution during tensile deformation was studied. When the engineering strain exceeded 0.4, austenite with high stability was retained, which required high stress to initiate martensitic transformation. Thus, only a small amount of austenite with high stability transformed to martensite after engineering strain 0.4 in Fig. 6(b).

Figure 7 shows the microstructure of 750 °C sample strained to 0.2 and 0.4, respectively. Comparing the deformed microstructure with the original microstructure (Fig. 1(b)), it is clear that ferrite was elongated at engineering strain 0.2 in Fig. 7(a), and majority of ferrite was bended and squeezed at

engineering strain 0.4 in Fig. 7(b). Thus, although a large fraction of austenite had transformed (as evidenced in Fig. 6b) in this stage, the local stress induced by transformed martensite was transferred and absorbed by the adjacent ferrite (Ref 26–28), leading to a slow increase in WH in stage 2.2 in Fig. 5(b). Moreover, this suggests that the superior ductility of 750 °C sample is not only related to the TRIP effect of austenite, but also to the cooperative deformation of ferrite. In contrast, 800 °C sample was characterized by low austenite stability, WH increased rapidly in stage 2 and retained a high value in stage 3, indicating that TRIP effect occurred during the initial stage of deformation, and quickly exhausted during deformation, leading to a lower TE but higher UTS.

4.2 Mechanical Property Difference in the Two Sets of Samples

Although the variation of tensile properties are similar in the two sets of samples, there are some difference between them. The comparison of tensile properties in the two groups of samples were summarized in Fig. 8. It is noted that YS of air-cooled samples is less than water-quenched samples, which is primarily attributed to recovery and grain growth. Moreover, the difference in the YS between the two groups decreases with increase in temperature (Fig. 8). To further analyze the influence of grain size on YS, the grain size (Figs. 1 and 2) were measured by Image Pro Plus analysis software and were summarized in Table 1. It is clear that the grain size of air-

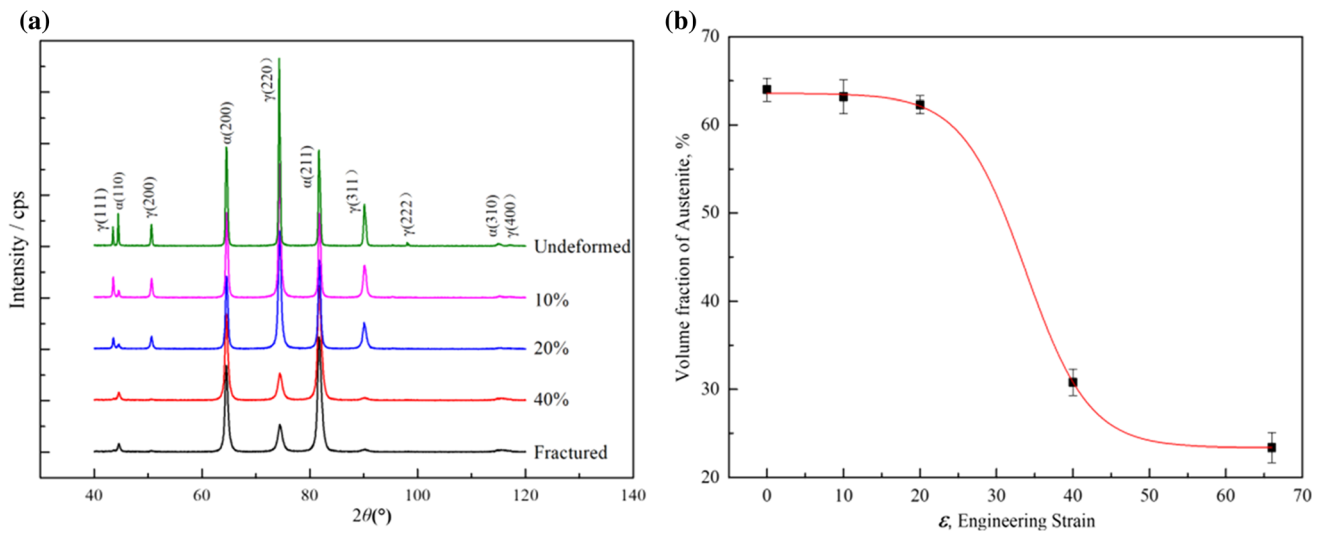


Fig. 6. XRD patterns of the sample water quenched from 750 °C. (a) and the volume fraction of austenite, (b) as a function of engineering strain

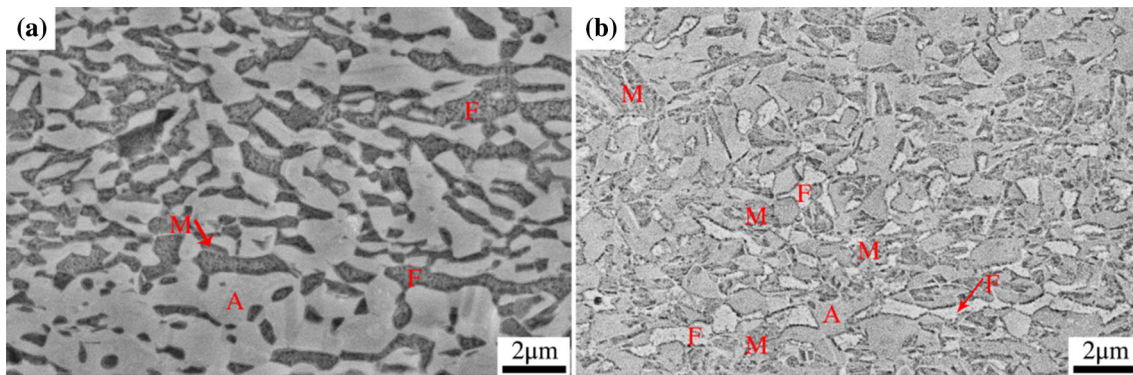


Fig. 7. SEM micrographs of the sample water quenched from 750 °C subjected to different strain. (a) at the strain of 0.2, (b) at the strain of 0.4

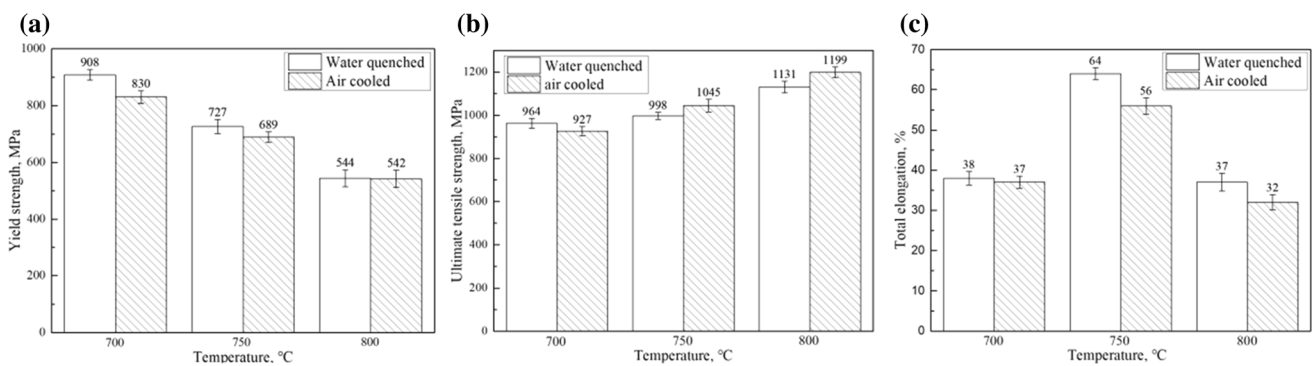


Fig. 8. Comparison of tensile properties in the two sets of samples. (a) yield strength, (b) ultimate tensile strength, (c) total elongation

cooled samples was larger than the water-quenched samples, and the difference in grain size between the two sets of samples decreased with increase in temperature, which led to decrease in YS in Fig. 8, consistent with the Hall–Petch equation (Ref 29).

The air-cooled samples demonstrate a lower TE than the water-quenched samples, which is probably attributed to the difference of austenite stability (Table 2). In the attempt to

compare the austenite stability of the two sets of samples, and to interpret their difference in tensile properties, the austenite stability was quantified by equation (Ref 30, 31):

$$\ln\left(\frac{f_y}{f_{y0}}\right) = -k\varepsilon \quad (\text{Eq 3})$$

Table 1. Grain size of ferrite and austenite at different annealing temperatures

Temperature, °C	Water-quenched samples			Air-cooled samples		
	700	750	800	700	750	800
Ferrite grain size, μm	0.34	0.53	0.72	0.50	0.65	0.73
Austenite grain size, μm	0.51	0.99	1.17	0.64	1.01	1.23

where f_γ , $f_{\gamma 0}$ and k are the austenite fraction at strain ε , the initial austenite fraction, and the mechanical stability of austenite, respectively. A higher k value is indicated lower austenite stability. According to Table 2, austenite stability decreases with the increase of annealing temperature. Combined Table 2 with Fig. 8, it is inferred that the air-cooled samples had a higher austenite stability than the water-quenched samples, which implied enhanced TRIP effect in water-quenched samples, contributing to higher elongation. However, it is intriguing that the UTS of air-cooled samples was greater than the samples water quenched from 750~800 °C.

The WH behavior of two sets of samples is illustrated in Fig. 9. The samples annealed at identical temperature had similar variation of WH. Combining Fig. 9 with Fig. 8b, it can be deduced that the greater WH is related to higher UTS. As shown in Fig. 9(b), 750 °C air-cooled sample has a higher WH than the water-quenched sample in stage 2, but lasted for a small strain. Fig. 10 shows the SEM microstructure of the two sets of samples after tensile fracture. It is apparent that ferrite was seriously squeezed and appeared to spill over in the samples water quenched from 750~800 °C. In contrast, in the air-cooled samples the deformation of ferrite was not apparent. It is inferred that the difference in ferrite behavior is related with fraction and stability of austenite. As shown in Fig. 3, the fraction of hard transformed martensite was less, but the fraction of soft austenite was larger in the air-cooled samples, leading to weaker stress concentration in ferrite. Based on the above mentioned discussion, TRIP effect and cooperative deformation of ferrite contributed to the superior TE in 750 °C water-quenched sample. Moreover, it is confirmed that TRIP effect without the cooperative deformation of ferrite in air-cooled sample contributed to UTS, and contributed less to TE. In addition, the cooperative deformation of ferrite which absorbed the stress induced by martensite (transformed from austenite) was responsible for the lower WH and UTS in the water-quenched samples. For 800 °C samples, as shown in Fig. 9(c), the WH increased rapidly in stage 1, indicating massive austenite transformed into martensite in the initial deformation stage, which was detrimental to the elongation of 800 °C sample. In contrast, although TRIP effect was insignificant in 700 °C sample (as evidenced in Fig. 3), the negative effect of martensite to elongation is much less than 800 °C sample, leading to a slightly higher elongation in 700 °C sample. Moreover, according to Fig. 9(c), the 800 °C air-cooled sample demonstrated a higher WH than the water-quenched sample. It is noted that the WH in stage 3 of 800 °C air-cooled sample decreased smoothly than that of water-quenched sample, indicating a deduced discontinuous TRIP effect.

The stability of austenite is mainly influenced by grain size, chemical elements, and morphology, etc. The grain size of austenite increased with increase of annealing temperature

Table 2. Mechanical stability of austenite as a function of temperature

	700 °C	750 °C	800 °C
Water-quenched samples	0.4	1.5	6.0
Air-cooled samples	0.3	1.3	2.8

(Table 1), which led to decrease in the stability of austenite (as implied by Table 2) (Ref 32, 33). In addition, the austenite grain morphology of 800 °C samples was mainly granular and blocky before tensile deformation (Figs. 1c and 2c). After tensile deformation, for 800 °C water-quenched samples, the granular austenite grain was retained, and the blocky austenite was transformed to martensite, because granular austenite had greater stability than blocky austenite (Fig. 10c). In contrast, for 800 °C air-cooled samples, the granular and blocky austenite both were hardly observed, and partial austenite in the vicinity of blocky austenite boundary and some lamellar austenite were retained (Fig. 10f). According to our previous work, the segregation of Mn and C could result in increase of austenite stability (Ref 32, 33). Thus, the retained austenite in Fig. 10f was attributed to partitioning of elements, which was further confirmed by EPMA. In addition, it is inferred that the air-cooled samples having a higher austenite stability than the water-quenched samples was attributed to partitioning of elements. The partitioning of elements in water-quenched samples was only active in the annealing heat preservation stage, due to very fast cooling rate. In contrast, the partitioning of elements in air-cooled samples was active both in the annealing heat preservation stage and cooling period, due to slow cooling rate.

As illustrated in Fig. 11, it is clear that austenite has a higher Mn and C concentration than ferrite. Moreover, Mn was distributed uniformly in the blocky austenite grains, while C was segregated in some blocky austenite boundaries and the lamellar austenite grains, which can improve austenite stability, accounting for the blocky austenite retained in the air-cooled sample (consistent with Fig. 11a). Therefore, it is suggested that the critical factor in controlling austenite stability of the water-quenched samples was morphology, while the dominant factor in austenite stability of the air-cooled samples was composition.

5. Conclusions

- (1) The grain size of austenite was increased with increase of annealing temperature, which led to decrease in austenite stability and yield strength. The samples an-

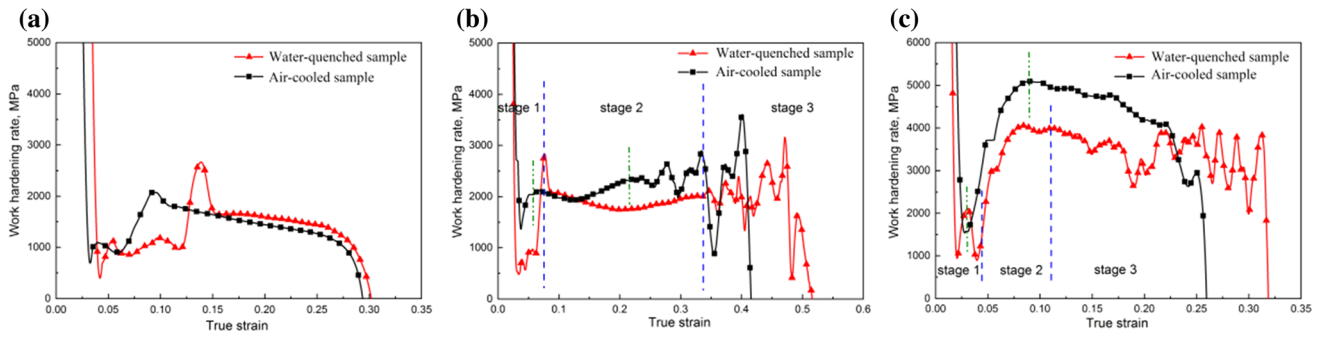


Fig. 9. Comparison of work hardening rate of the two sets of samples annealed at different temperatures. (a) 700 °C, (b) 750 °C, (c) 800 °C

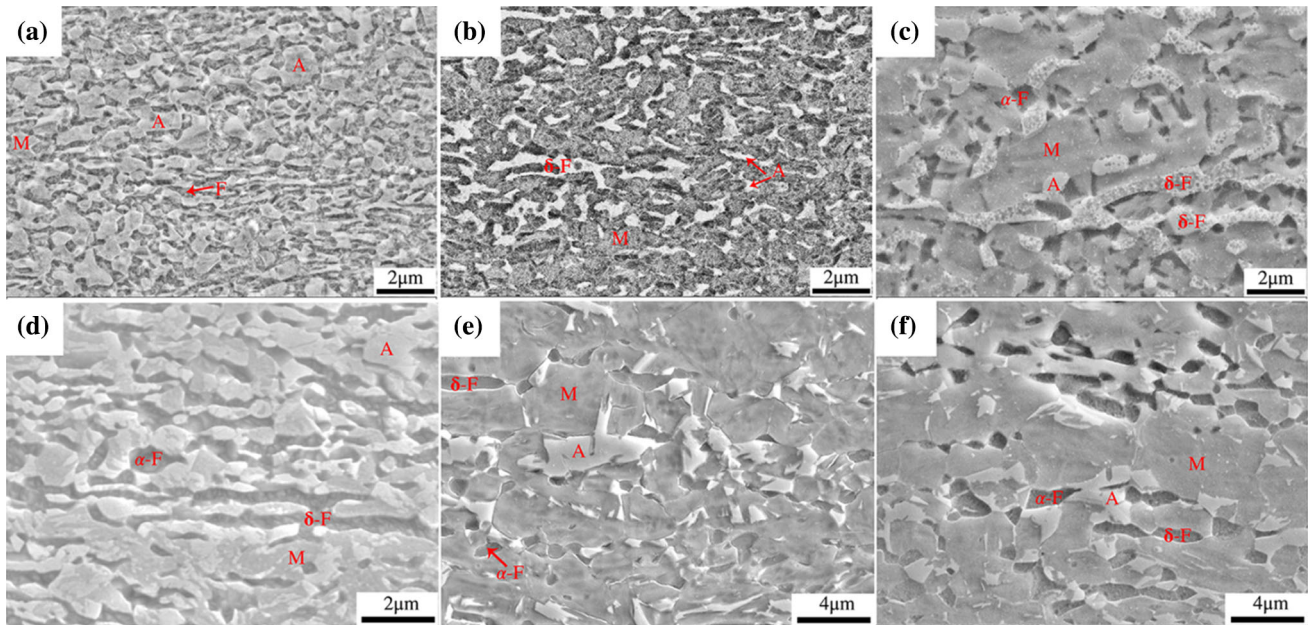


Fig. 10. SEM micrographs of the two sets of samples after tensile fractured. Corresponding to the samples water quenched from 700, 750, and 800 °C (a, b, c), respectively, and (d, e, f) samples air cooled from 700 °C, 750 °C, and 800 °C, respectively

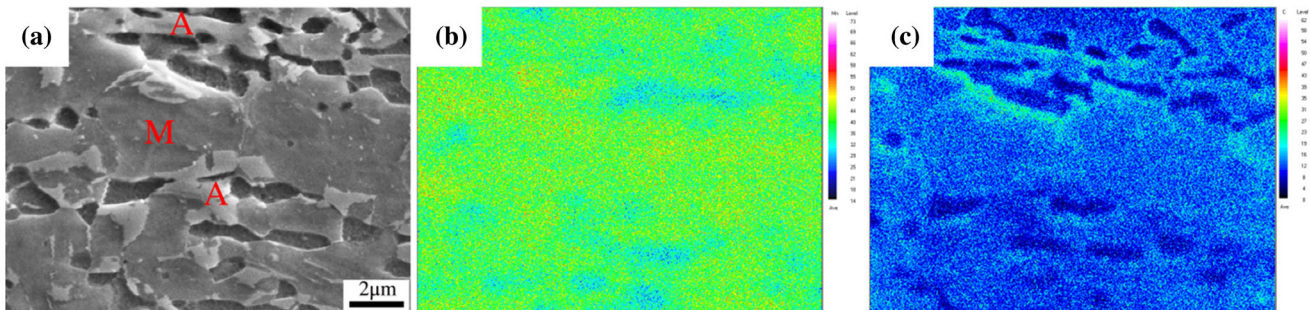


Fig. 11. SEM micrograph (a) of the sample air cooled from 800 °C after tensile fracture, (b) and (c) are the corresponding Mn and C concentration by EPMA, respectively

annealed at 750 °C, whether water quenched or air cooled, had a medium austenite stability, and demonstrated significantly higher ductility compared to samples annealed at 700 and 800 °C. The superior TE in 750 °C sample is related to the cumulative contribution of TRIP effect of austenite and the cooperative deformation of ferrite.

(2) The air-cooled samples were characterized by higher austenite stability and UTS, but lower TE as compared

to the water-quenched samples. It is suggested that TRIP effect without the cooperative deformation of ferrite in air-cooled sample primarily contributed to WH and UTS, but contributed less to TE. In contrast, the cooperative deformation of ferrite which absorbed the stress induced by martensite (transformed from austenite) was responsible for lower WH and UTS in the water-quenched samples.

- (3) In the case of samples annealed at 800 °C, after tensile fracture, the retained austenite of water-quenched sample was granular, and the blocky austenite disappeared. In contrast, in the air-cooled sample, some blocky austenite was still retained because of enrichment of Mn and C. Thus, the critical factor in controlling austenite stability of water-quenched sample was morphology, granular austenite showing the highest stability; while the dominant factor in austenite stability of the air-cooled sample was composition, enrichment of Mn and C improving austenite stability.

Acknowledgments

The authors acknowledge support from the National Natural Science Foundation of China (51974084), Taiyuan University of Science and Technology Scientific Research Initial Funding (20202039), China Postdoctoral Science Foundation (2020M673194 and 2020T130329). The authors sincerely thank R.D.K. Misra for guidance in the study and significant contribution to the discussion.

References

- H.W. Luo, J. Shi, C. Wang, W.Q. Cao, X.J. Sun and H. Dong, Experimental and Numerical Analysis on Formation of Stable Austenite during the Intercritical Annealing of 5Mn Steel, *Acta Mater.*, 2011, **59**(10), p 4002–4014
- J. Hu, J.M. Zhang, G.S. Sun, L.X. Du, Y. Liu, Y. Dong and R.D.K. Misra, High Strength and Ductility Combination in Nano-/ Ultrafine-Grained Medium-Mn steel by Tuning the Stability of Reverted Austenite Involving Intercritical Annealing, *J. Mater. Sci.*, 2019, **54**, p 6565–6578
- B.H. Sun, K. Waldemar, R. Michael, D. Ponge and D. Raabe, Dependence of Hydrogen Embrittlement Mechanisms on Microstructure-driven Hydrogen Distribution in Medium Mn Steels, *Acta Mater.*, 2020, **183**(15), p 313–328
- J. Hu, L.X. Du, Y. Dong, Q.W. Meng and R.D.K. Misra, Effect of Ti Variation on Microstructure Evolution and Mechanical Properties of Low Carbon Medium Mn Heavy Plate Steel, *Mater. Charact.*, 2019, **152**, p 21–35
- H. Lee, M.C. Jo, S.S. Sohn, A. Zargarani, J.H. Ryuc, N.J. Kim and S. Lee, Novel Medium-Mn (Austenite+Martensite) Duplex Hot-rolled Steel Achieving 1.6 GPa Strength with 20% Ductility by Mn-Segregation-induced TRIP Mechanism, *Acta Mater.*, 2018, **147**, p 247–260
- Z.H. Cai, B. Cai, H. Ding, Y. Chen and R.D.K. Misra, Microstructure and Deformation Behavior of the Hot-rolled Medium Manganese Steels with Varying Aluminum-content, *Mater. Sci. Eng. A*, 2016, **676**, p 263–270
- B. Kim, J. Sietsma and M.J. Santofimia, The Role of Silicon in Carbon Partitioning Processes in Martensite/austenite Microstructures, *Mater. Des.*, 2017, **127**, p 336–345
- J. Wang and S.V.D. Zwaag, Stabilization Mechanisms of Retained Austenite in Transformation-induced Plasticity Steel, *Metall. Mater. Trans. A*, 2001, **32A**, p 1527–1539
- A. Garcia-Junceda, C. Capdevila, F.G. Caballero and C. Garcíade-Andrés, Dependence of Martensite Start Temperature on Fine Austenite Grain Size, *Scr. Mater.*, 2008, **58**(2), p 134–137
- X.C. Xiong, B. Chen, M.X. Huang, J.F. Wang and L. Wang, The Effect of Morphology on the Stability of Retained Austenite in a Quenched and Partitioned Steel, *Scr. Mater.*, 2013, **68**(5), p 321–324
- K. Sugimoto, M. Misu, M. Kobayashi and H. Shirasawa, Effects of Second Phase Morphology on Retained Austenite Morphology and Tensile Properties in a TRIP-aided Dual-phase Steel Sheet, *ISIJ Int.*, 1993, **33**, p 775–782
- C.H. Seo, K.H. Kwon, K. Choi, K.H. Kim, J.H. Kwak, S. Lee and N.J. Kim, Deformation Behavior of Ferrite-austenite Duplex Light Weight Fe-Mn-Al-C Steel, *Scr. Mater.*, 2012, **66**(8), p 519–522
- Z.H. Cai, H. Ding, X. Xue and Q.B. Xin, Microstructural Evolution and Mechanical Properties of Hot-rolled 11% Manganese TRIP Steel, *Mater. Sci. Eng. A*, 2013, **56**, p 388–395
- Z.C. Li, H. Ding, R.D.K. Misra and Z.H. Cai, Microstructure-mechanical Property Relationship and Austenite Stability in Medium-Mn TRIP steels: The Effect of Austenite-reverted Transformation and Quenching-tempering Treatments, *Mater. Sci. Eng. A*, 2017, **682**, p 211–219
- J. Han, S.J. Lee, J.G. Jung and Y.K. Lee, The Effects of the Initial Martensite Microstructure on the Microstructure and Tensile Properties of Intercritically Annealed Fe-9Mn-0.05 C Steel, *Acta Mater.*, 2014, **78**, p 369–377
- M. Soleimani, A. Kalhor and H. Mirzadeh, Transformation-induced Plasticity (TRIP) in Advanced Steels: A Review, *Mater. Sci. Eng. A*, 2020, **795**, p 140023.
- Z.H. Cai, H. Ding, R.D.K. Misra, H. Kong and H.Y. Wu, Unique Impact of Ferrite in Influencing Austenite Stability and Deformation Behavior in a Hot-rolled Fe-Mn-Al-C Steel, *Mater. Sci. Eng. A*, 2014, **595**, p 86–91.
- J. Han and Y.K. Lee, The Effects of the Heating Rate on the Reverse Transformation Mechanism and the Phase Stability of Reverted Austenite in Medium Mn Steels, *Acta Mater.*, 2014, **67**, p 354–361.
- K. Steineder, R. Schneider, D. Krizan, C. Béal and C. Sommitsch, Comparative Investigation of Phase Transformation Behavior as a Function of Annealing Temperature and Cooling Rate of Two Medium-Mn Steels, *Steel Res. Int.*, 2015, **86**(10), p 1179–1186.
- Z.H. Cai, H. Ding, X. Xue, J. Jiang, Q.B. Xin and R.D.K. Misra, Significance of Control of Austenite Stability and Three-stage Work-hardening Behavior of an Ultrahigh Strength-high Ductility Combination Transformation-induced Plasticity Steel, *Scr. Mater.*, 2013, **68**(11), p 865–868.
- A.K. Srivastava, D. Bhattacharjee, G. Jha, N. Gope and S.B. Singh, Microstructural and Mechanical Characterization of C-Mn-Al-Si Cold-rolled TRIP-aided Steel, *Mater. Sci. Eng. A*, 2007, **445A**(46), p 549–557.
- Z.H. Cai, H.Y. Li, S.Y. Jing, Z.C. Li, H. Ding, Z.Y. Tang and R.D.K. Misra, Influence of Annealing Temperature on Microstructure and Tensile Property of Cold-rolled Fe-02C-11Mn-6Al Steel, *Mater. Charact.*, 2018, **137**, p 256–262.
- N. Nakadaa, K. Mizutani, T. Tsuchiyama, S. Takaki, Difference in Transformation Behavior between Ferrite and Austenite Formations in Medium Manganese Steel, *Acta Materialia.*, 2014, **65**, p 251–258
- Z. Wang, J.P. Xu and J.X. Li, Mechanical Properties and Fracture Behaviors of Medium-Mn Steels with and without Delta-ferrite for Different Intercritical Annealing Times, *Mater. Charact.*, 2021, **172**, p 110730.
- Z.H. Cai, H. Ding, R.D.K. Misra and H. Kong, Unique Serrated Flow Dependence of Critical Stress in a Hot-rolled Fe-Mn-Al-C Steel, *Scr. Mater.*, 2014, **71**, p 5–8.
- F.Y. Xu, B.Z. Bai and H.S. Fang, Influences of Volume Fraction, Shape and Strength of Martensite Islands on Mechanical Properties of Granular Structure Steels, *Acta Metall. Sin.*, 2008, **44**, p 1183–1187.
- T.Y. Cao, Study on Relationship Between Properties and Martensite Content and Size of Dual-phase Steel, *Res. Iron Steel*, 2006, **34**, p 24–27.
- K.W. Zhao, Q. Ma, H.X. Zhang and J. Wang, Effect of Recrystallization Annealing Temperature on Microstructure of Cold Deformation Duplex Stainless Steel 00Cr22Ni5M3No, *Mater. Heat Treat.*, 2009, **38**, p 107–109.
- J. Zhou, Thoughts on Teaching of Fine-grained Strengthening in Metallurgy, *Educ Teach Forum*, 2017, **2**, p 192–193.
- S. Zhou, K. Zhang, Y. Wang, J.F. Gu and Y.H. Rong, High Strength-elongation Product of Nb-microalloyed Low-carbon Steel by a Novel Quenching-Partitioning- Tempering Process, *Mater. Sci. Eng. A*, 2011, **528**(27), p 8006–8012.
- S. Zhang and K.O. Findley, Quantitative Assessment of the Effects of Microstructure on the Stability of Retained Austenite in TRIP Steels, *Acta Mater.*, 2013, **61**, p 1895–1903.
- Z.H. Cai, H. Ding, R.D.K. Misra and Z.Y. Ying, Austenite Stability and Deformation Behavior in a Cold-rolled Transformation-induced Plas-

ticity Steel with Medium Manganese Content, *Acta Mater.*, 2015, **84**, p 229–236.

33. Z.C. Li, R.D.K. Misra, Z.H. Cai, H.X. Li and H. Ding, Mechanical Properties and Deformation Behavior in Hot-rolled 02C–15/3Al–8.5Mn–Fe TRIP Steel: The Discontinuous TRIP Effect, *Mater. Sci. Eng. A*, 2016, **673**, p 63–72.

Publisher's Note Springer Nature remains neutral with regard to jurisdictional claims in published maps and institutional affiliations.